An InSAR-based survey of volcanic deformation in the southern Andes

M. E. Pritchard
Department of Geosciences, Princeton University, Princeton, New Jersey, USA

M. Simons
Seismological Laboratory, Division of Geological and Planetary Sciences, California Institute of Technology, Pasadena, California, USA

Received 18 May 2004; revised 30 June 2004; accepted 8 July 2004; published 6 August 2004.

[1] We use Interferometric Synthetic Aperture Radar (InSAR) to search for surface deformation in the southern Andes (40°S–46°S and 49°S–53°S) associated with magmatic processes. Although the available data are not optimal, we can constrain the amount of volcanic deformation at about 27 Holocene volcanoes between the years 1993–1999. We detect inflation of Cerro Hudson volcano following its 1991 eruption, and use spherical and non-spherical models to constrain the source of deformation to be between 4 and 8 km below sea level. We measure the rate of deformation to be about 5 cm/year in the radar line-of-sight, and infer that the maximum deformation could exceed 10 cm/year in the center of the caldera. Within the errors of the measurements, the rate of deformation is constant from 1993–1998 ($10–30 \times 10^6$ m^3/year). At this rate, 100–200 years is required to accumulate the volume of material erupted in 1991. *INDEX TERMS:* 1243 Geodesy and Gravity: Space geodetic surveys; 8145 Tectonophysics: Physics of magma and magma bodies. **Citation:** Pritchard, M. E., and M. Simons (2004), An InSAR-based survey of volcanic deformation in the southern Andes, *Geophys. Res. Lett.*, *31*, L15610, doi:10.1029/2004GL020545.

1. Introduction

[2] In the southern Andes, volcanism occurs in two distinct regions (Figure 1): the Southern Volcanic Zone (SVZ – north of the Nazca-South America-Antarctica triple junction from 33°S–46°S), and the Austral Volcanic Zone (AVZ – south of the triple junction from 49°S–55°S). The SVZ has had about as many historical eruptions as the central and northern Andean volcanic zones combined, and encompasses perhaps 1,334 eruptive centers [*Gonzalez-Ferran*, 1995], with about 60 active in the Holocene [*Simkin and Siebert*, 1994]. The AVZ has seven recognized volcanoes, although their activity is poorly constrained because of their remoteness.

[3] While the most active volcanoes in this region (Llaima and Villarica) and a few others are monitored by the Southern Andes Volcano Observatory (OVDAS), the activity of most volcanoes is not well-known. Here, we determine where existing satellite based repeat-pass InSAR data can be used to monitor activity in the SVZ and AVZ, place constraints on the recent rate of deformation of about 27 Holocene volcanoes, and report previously undocumented deformation at Cerro Hudson volcano, and possible deformation at Cordon Caulle.

2. Data Quality

[4] For InSAR to successfully measure surface deformation, the radar scattering properties of the ground can not change significantly between observations (in other words, the radar signal coherence must be high). To achieve high coherence in regions with significant snowfall such as the SVZ and AVZ, radar images must be acquired during the summer season (December–May). In addition, to make a quality interferogram from two SAR images, the satellite viewing geometry must be nearly identical in both acquisitions (i.e., the satellite baseline must be small). There is limited existing data that satisfy these requirements. We searched archives from all possible satellites (ERS-1/2, JERS and RADARSAT-1), and were only able to find usable data (spanning several years) from 40°S–46°S of the SVZ for the ERS-1/2 satellites. Data is available for the southern part of the SVZ in the summer season because this region is within sight of the O'Higgins (German) Antarctica downlink station (other nearby stations collected less data). Our attempts to try data slightly outside the seasonal constraint (in southern spring) or with baselines greater than 150 m within other parts of the arc were unsuccessful (Table 1 of auxiliary material[1]). Within the AVZ, there is much more data, and we only looked at a subset between 49°S–53°S.

[5] We use the Caltech/JPL ROI_PAC software for data processing [*Rosen et al.*, 2004] and test the SNAPHU program for unwrapping [*Chen and Zebker*, 2002]. Digital Elevation Models from the Shuttle Radar Topography Mission with 90 m pixel spacing are used to remove the topographic signature from the InSAR phase [*Farr and Kobrick*, 2000].

[6] A map of radar coherence within our study area is shown in Figure 1. For timespans of a year or more, coherence is generally low, even when the seasonal and baseline constraints are met, except on lava flows or rocky areas (especially on the Taitao peninsula). Because of the young lava flows at most of the Holocene volcanoes, successful measurements of the phase are possible at many locations. Observations are usually restricted to the volcano flanks and sometimes limited to only one side of the edifice.

0094-8276/04/2004GL020545$05.00

[1] Auxiliary material is available at ftp://ftp.agu.org/apend/gl/2004GL020545.

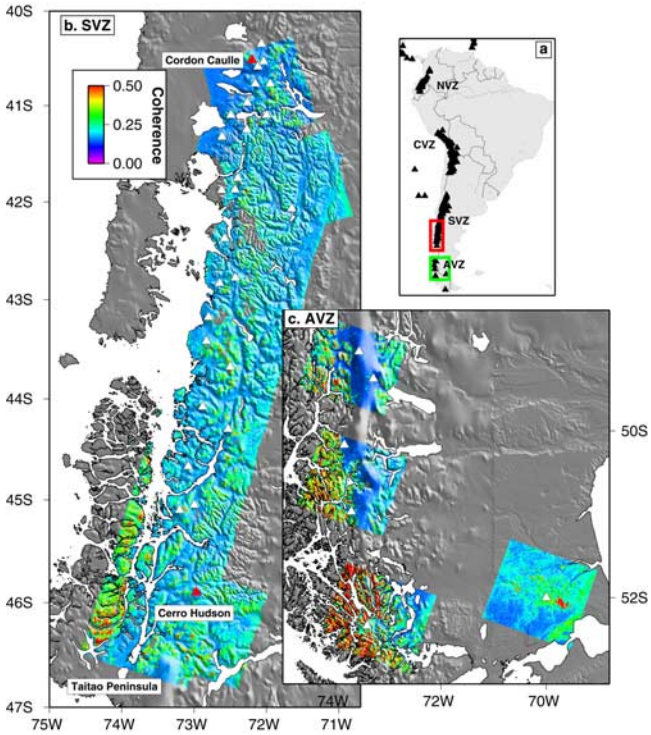

Figure 1. a. Reference map, with the red and green boxes indicating the areas shown in panels b. and c., respectively. b. Interferometric coherence from ERS (C-band, 5.7 cm wavelength) for the area where we have studied volcanic deformation in the SVZ. Interferograms span from 1996–1998/1999, starting and ending in February or March (complete list in Table 1 of the auxiliary material). We observe good interferometric coherence in rocky areas (like the Taitao Peninsula), but poorer coherence inland. Triangles are Holocene volcanoes, with Cerro Hudson and Cordon Caulle shown in red. c. Coherence in the AVZ, with same symbols as b. With the exception of the easternmost track, interferograms span January–March 1996–February 1999 (Table 1 of auxiliary material).

Coherence is broadly higher in the AVZ than the SVZ, where the vegetation is less lush.

3. Results

3.1. Deformation at Cerro Hudson

[7] Cerro Hudson is a remote ice-filled caldera about 10 km in diameter, and is one of the most active volcanoes in the southern Andes with at least 12 eruptions in the Holocene [e.g., *Naranjo and Stern*, 1998]. Hudson last erupted in August, 1991, ejecting as much as 7.6 km^3 of material (2.7 km^3 dense rock equivalent) [e.g., *Scasso et al.*, 1994]. The eruption was followed by several small phreatic explosions or subglacial melting episodes (http://www.volcano.si.edu).

[8] At Hudson, we observe the InSAR phase on the rocky slopes surrounding the caldera, and at the base of the Huemules glacier, but not within the caldera (Figure 2). We have made 15 interferograms from three orbital tracks, and found 10 of them from two different tracks maintain coherence near Hudson, and yield deformation in the same direction. We measure a portion of the deformation field (which presumably extends inside the caldera, where it could possibly become complex [e.g., *Amelung et al.*, 2000]), with a maximum inflation rate of about 5 cm/yr in the radar line-of-site (LOS). While many scenes have atmospheric contamination (there is a correlation between topography and phase at volcanic and non-volcanic peaks), using the criteria of *Pritchard and Simons* [2004], we think that most of the signal at Cerro Hudson is surface deformation. For example, correlation between phase and topography is opposite in sign at Hudson relative to nearby mountains.

[9] We assume that the deformation is caused by a volume change caused by an injection of magmatic or hydrothermal fluids, or by warming or melting of the crust. We model the deformation with both spherical and non-spherical sources of volume change in order to explore the range of models that explain the data. We use the same models and inversion strategy of *Pritchard and Simons* [2004]: a spherical point-source, a nearly vertical or horizontal prolate point-source [we fix the semi-major axis to be 1 km,] [*Yang et al.*, 1988], and a point-like or finite sized sill [*Fialko et al.*, 2001]. The different source shapes effect the inferred depth and volume of the source [e.g., *Dieterich and Decker*, 1975], and it is difficult to differentiate between the geometries with the limited InSAR data available.

[10] To model the deformation, we must unwrap the phase measurements (since interferograms only measure phase between 0 and 2π). Because our observations of the deformation field are discontinuous, it is not always obvious how to relate the phase of isolated patches. While the SNAPHU unwrapper chooses one way to connect the fragments, we solve for the integer number of phase cycles between fragments as part of our inversions. For most of the interferograms, there are only two or three isolated patches.

[11] In the inversions, we use two interferograms to estimate the source location, and then assume the geometry fixed for the other eight interferograms. We solve for the volume change, absolute offset of the phase relative to zero deformation, and the integer offset between isolated patches. For the spherical source, we find a depth of about 5 km below sea level. Given the low relief of Hudson (mean value about 900 m above sea level) and the depth of the source, calculations that include the effects of local topography [e.g., *Williams and Wadge*, 1998] show no significant

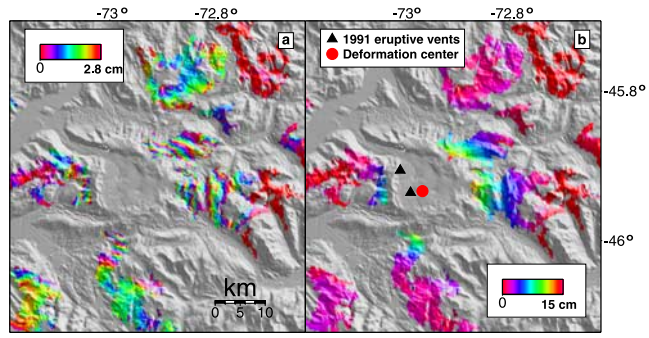

Figure 2. a. Wrapped interferogram at Cerro Hudson between 3 March 1996–22 February 1999. b. Unwrapped interferogram. The RMS difference between this data and a spherical model is 1.4 cm.

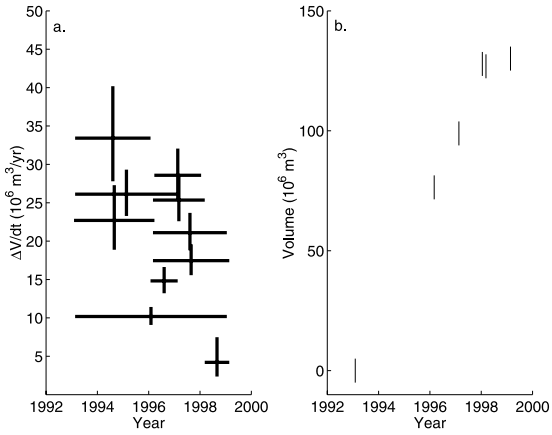

Figure 3. a. Inferred rate of volume change as a function of time, assuming a constant source depth, a spherical source in a half-space, and a constant rate of deformation during the time period covered in the interferogram. The horizontal bar shows the time period covered by the interferogram and the vertical bar reflects an estimate of the error on the inferred rate of volume change. The vertical error bar is estimated from inversions using different patches of unwrapped data. b. Volume inferred to be in the magma chamber as a function of time, assuming zero volume at the time of the first SAR image. Using the overlapping interferograms, we estimate the rate of deformation between each pair of SAR images with a linear least squares inversion, where pairs separated by 35 days or less are combined into a single observation. We plot the result as the cumulative volume within the source at the time of each SAR image. We assume a constant error for each measurement of 5×10^6 m^3.

effect on estimates of the source depth. The RMS difference between the data and the model is between 1–1.5 cm for most interferograms, which is higher than in other areas such as the central Andes [*Pritchard and Simons*, 2002] and consistent with the lower coherence. The center of the deformation pattern is located about 2–4 km from the 1991 eruptive vents [*Naranjo et al.*, 1993, Figure 2] which is not uncommon [*Pritchard and Simons*, 2004]. The non-spherical source depths range from about 4 km below sea level for a vertical prolate source, to about 8 km below sea level for a point crack. The spread in depth estimates as a function of assumed model geometry is as expected [e.g., *Pritchard and Simons*, 2004], but because only a portion of the deformation field is sampled, for any given geometry, the location and depth parameters are only known to a few kilometers.

[12] Between 1993–1998, there is a roughly constant rate of inflation of about $10–30 \times 10^6$ m^3/year (assuming a spherical model at 5 km depth). Inflation may have slowed or stopped between 1998–1999, although because we have only one usable interferogram spanning this interval, the error bounds are larger (Figure 3). There is no obvious evidence for an exponential reduction in the inflation rate following the 1991 eruption as observed following some other eruptions [e.g., *Dvorak and Dzurisin*, 1997].

3.2. Deformation at Cordon Caulle

[13] We observe possible subsidence in a region called Cordon Caulle (Figure 1 and figure in auxiliary material), a 17 km long, 2.5 km wide zone of volcanic fissures, domes and craters between the Cordillera Nevada caldera and the Puyehue volcano [e.g., *Gerlach et al.*, 1988]. We are less certain of this measurement because only a single interferogram can be made of this area. However, the signal does not look like the atmospheric contamination in other areas (e.g., the phase is not correlated with topography), and the amplitude is several cm, larger than other obvious atmospheric artifacts we observe. There have been several eruptions at different locations within this region during the 19th and 20th centuries, with the most recent occurring 2 days after the great 1960 Chilean earthquake [*Gonzalez-Ferran*, 1995]. Currently there is hydrothermal activity at Cordon Caulle, and shallow earthquakes have been reported [*Smithsonian Institution*, 1994]. We have not attempted to model the observations because the limited spatial extent of the phase limits our ability to resolve the depth of the source [e.g., *Masterlark and Lu*, 2004], but the deformation pattern is clearly non-spherical and non-axisymmetric, and so a distribution of sources are probably necessary.

3.3. Upper Limits on Deformation

[14] Although none of the 27 volcanoes we can survey with InSAR erupted during the period of observation, these volcanoes are still active: seven have erupted this century and another five have historic eruptions (http://www.volcano.si.edu). Because many of these volcanoes have young lava flows covering at least half of the edifice and extending for some distance down the flanks, constraints can be made upon the rate of deformation and the amount of magma moving at depth. In fact, many of these volcanoes have superior coherence to Hudson (and better azimuthal coverage), so the fact that deformation is seen at Hudson, but not clearly at any other volcano sets an upper limit of 3 cm/year at these volcanoes. At some volcanoes, we can set even lower constraints on the rate of deformation (Table 2 of auxiliary material). Translating the rate of deformation to a depth and volume change of a magma chamber is not unique because it depends on the geometry of the magma source, but we can get an order of magnitude estimate if we assume a spherical source [e.g., *Pritchard and Simons*, 2004, Figure 11]. For example, if the source depth is shallower than 10 km, less than 1×10^7 m^3/year of magma is moving beneath most of these volcanoes during the time period of our observations.

4. Conclusions

[15] With InSAR, entire volcanic arcs can be surveyed, and magma is found to be moving beneath many volcanoes with no other signs of activity [*Amelung et al.*, 2000; *Wicks et al.*, 2002; *Lu et al.*, 2000, 2002; *Pritchard and Simons*, 2002]. Even in regions that are not ideal for InSAR (southern Andes, Alaska), useful constraints on volcanic activity are possible when observations are frequent in the summer and the baselines are well-controlled [e.g., *Lu and Freymueller*, 1998]. Therefore, a global census of all the world's subaerial volcanoes is possible with the properly designed spacecraft mission, and these studies can isolate areas for future study, like Cerro Hudson and Cordon Caulle.

[16] **Acknowledgments.** We thank two anonymous referees for comments and R. B. Lohman, Y. Fialko, and L. Rivera for modeling software.

ERS SAR imagery was acquired under a Category 1 research project from the European Space Agency. The GMT program was used to create several figures [*Wessel and Smith*, 1998]. M.E.P. was partly supported by a Hess postdoctoral fellowship from Princeton University. Contribution number 9081 of the Division of Geological and Planetary Science, Seismological Laboratory, California Institute of Technology.

References

Amelung, F., S. Jónsson, H. Zebker, and P. Segall (2000), Widespread uplift and 'trapdoor' faulting on Galápagos volcanoes observed with radar interferometry, *Nature*, *407*, 993–996.

Chen, C. W., and H. A. Zebker (2002), Phase unwrapping for large SAR interferograms: Statistical segmentation and generalized network models, *IEEE Trans. Geosci. Remote Sens.*, *40*, 1709–1719.

Dieterich, J., and R. Decker (1975), Finite element modeling of surface deformation associated with volcanism, *J. Geophys. Res.*, *80*, 4094–4102.

Dvorak, J. J., and D. Dzurisin (1997), Volcano geodesy: The search for magma reservoirs and the formation of eruptive vents, *Rev. Geophys.*, *35*, 343–384.

Farr, T. G., and M. Kobrick (2000), Shuttle Radar Topography Mission produces a wealth of data, *Eos Trans. AGU*, *81*(48), 583–585.

Fialko, Y., Y. Khazan, and M. Simons (2001), Deformation due to a pressurized horizontal circular crack in an elastic half-space, with applications to volcano geodesy, *Geophys. J. Int.*, *146*, 181–190.

Gerlach, D. C., F. A. Frey, and R. H. M. López-Escobar (1988), Recent volcanism in the Puyehue Cordon-Caulle region, southern Andes, Chile (40.5°S): Petrogenesis of evolved lavas, *J. Petrol.*, *29*, 333–382.

Gonzalez-Ferran, O. (1995), *Volcanes de Chile* (in Spanish), Inst. Geogr. Mil., Santiago.

Lu, Z., and J. Freymueller (1998), Synthetic aperture radar interferometry coherence analysis over Katmai volcano group, Alaska, *J. Geophys. Res.*, *103*, 29,887–29,894.

Lu, Z., J. C. Wicks, D. Dzurisin et al. (2000), Aseismic inflation of Westdahl volcano, Alaska, revealed by satellite radar interferometry, *Geophys. Res. Lett.*, *27*, 1567–1570.

Lu, Z., J. C. Wicks, D. Dzurisin et al. (2002), Magmatic inflation at a dormant stratovolcano: 1996–1998 activity at Mount Peulik volcano, Alaska, revealed by satellite radar interferometry, *J. Geophys. Res.*, *107*(B7), 2134, doi:10.1029/2001JB000471.

Masterlark, T., and Z. Lu (2004), Transient volcano deformation sources imaged with interferometric synthetic aperture radar: Application to Seguam Island, Alaska, *J. Geophys. Res.*, *109*, B01401, doi:10.1029/2003JB002568.

Naranjo, J. A., and C. Stern (1998), Holocene explosive activity of Hudson volcano, southern Andes, *Bull. Volcanol.*, *59*, 291–306.

Naranjo, J., H. Moreno, and N. G. Banks (1993), La erupción del volcán Hudson en 1991 (46°S), XI Región, Aisén, Chile, in *Serv. Nac. Geol. Min. Bol.*, *44*, 50.

Pritchard, M. E., and M. Simons (2002), A satellite geodetic survey of large-scale deformation of volcanic centres in the central Andes, *Nature*, *418*, 167–171.

Pritchard, M. E., and M. Simons (2004), An InSAR-based survey of volcanic deformation in the central Andes, *Geochem. Geophys. Geosys.*, *5*, Q02002, doi:10.1029/2003GC000610.

Rosen, P. A., S. Hensley, G. Peltzer, and M. Simons (2004), Updated Repeat Orbit Interferometry Package released, *Eos Trans. AGU*, *85*(5), 47.

Scasso, R. A., H. Corbella, and P. Tiberi (1994), Sedimentological analysis of the tephra from the 12–15 August 1991 eruption of Hudson volcano, *Bull. Volcanol.*, *56*, 121–132.

Simkin, T., and L. Siebert (1994), *Volcanoes of the World*, Geosci. Press, Tucson, Ariz.

Smithsonian Institution (1994), Cordon Caulle, *Bull. Global Volcanism Network*, *19*(5), XX–XX.

Wessel, P., and W. H. F. Smith (1998), New, improved version of the Generic Mapping Tools released, *Eos Trans. AGU*, *79*(47), 579. [version 3.1]

Wicks, C. W., Jr., D. Dzurisin, S. Ingebritsen et al. (2002), Magmatic activity beneath the quiescent Three Sisters volcanic center, central Oregon Cascade Range, USA, *Geophys. Res. Lett.*, *29*(7), 1122, doi:10.1029/2001GL014205.

Williams, C. A., and G. Wadge (1998), The effects of topography on magma chamber deformation models: Application to Mt. Etna and radar interferometry, *Geophys. Res. Lett.*, *25*, 1549–1552.

Yang, X.-M., P. M. Davis, and J. H. Dieterich (1988), Deformation from inflation of a dipping finite prolate spheroid in an elastic half-space as a model for volcanic stressing, *J. Geophys. Res.*, *93*, 4249–4257.

M. E. Pritchard, Department of Geosciences, Guyot Hall, Princeton University, Princeton, NJ 08544, USA. (matt@princeton.edu)

M. Simons, Seismological Laboratory, Division of Geological and Planetary Sciences, California Institute of Technology, MC 252-21, Pasadena, CA 91125, USA.